

A systematic search for high surface brightness giant arcs in the Sloan Digital Sky Survey

S. Allam¹, J. Annis¹, H.T. Diehl¹, J. Estrada¹, P. B. Hall², T. Las¹, H. Lin¹, M. Makler³, K. W. Merritt¹, V. Scarpine¹ and D. Tucker¹.

¹ *Fermi National Accelerator Laboratory, Illinois, USA*

² *Department of Physics and Astronomy, York University, 4700 Keele St., Toronto, Ontario, M3J 1P3, Canada*

³ *Centro Brasileiro de Pesquisas Fisicas, Rio de Janeiro, Brazil*

ABSTRACT

We present the results of an arc search in a sample of SDSS galaxy clusters. A total of 825 clusters were studied and no gravitational arcs are detected. We present a selection function for our survey in the form of efficiency of detection curves as a function of arc parameters for a visual inspection of the images and for an automated search. The selection function is such that we are sensitive only to long high surface brightness arcs: $\mu_g \leq 24.8$ and $l/w \geq 10$. The results are interpreted as an upper limit in the arc probability per cluster. Our upper limits are compatible with previous arc searches. Lastly, we report on a serendipitous discovery of a giant arc in the SDSS data, known inside the SDSS Collaboration as Hall's arc.

1. Introduction

Clusters of galaxies are recognized as the largest virialized structures in the Universe, containing a large fraction of the dark matter in the Universe. Because they constitute a good probe for cosmology, understanding them in detail has been a major field of research. Strong gravitational lensing by the cluster of background galaxies is one such probe of the structure of clusters. Strong lensing has been observed in previous work, with the most extreme case being the giant gravitational arcs first seen in 1986 (Lynds & Petrosian 1989). There have been many surveys for arcs since then, including the search around x-ray luminous clusters (Luppino et al. 1999), in HST images of cluster centers (Sand et al. 2005), and in optical cluster catalogs from LCDCS (Zaritsky & Gonzalez 2003) and the RCS (Gladders et al. 2003).

Comparison of the abundance of gravitational arcs with theoretical predictions has been proposed as a tool to constrain cosmology (Bartelmann et al. 1998). The early results indicated that the number of strongly-lensed arcs greatly exceeded that expected from Λ CDM simulations. More detailed study of the systematic effects involved in this analysis seem to indicate that the observations do, in fact, agree with the theoretical expectations from the standard cosmology (Dalal et al. 2004; Wambsganss et al. 2004; Oguri et al. 2003). The main goal of the work presented here is not in the extraction of cosmological information from the statistics of gravitational arcs. Instead it is to both a) locate high surface brightness, giant arcs that would prove useful in followup programs aimed at tests such as outlined by Gilmore & Natarajan (2006), and more directly here b) understanding the probability for a galaxy cluster to produce a giant arc as a function of its mass and redshift. We believe this is an important aspect to be considered before cosmology can be extracted from arcs statistics and that it will provide a significant improvement in our understanding of the mass distribution inside galaxy clusters.

A defining characteristic of previous arc searches is that the search is done in the most massive clusters. Luppino et al. (1999) searched for arcs in 38 x-ray selected clusters ($0.15 \leq z \leq 0.82$) with $L_x \geq 2 \times 10^{44}$ ergs/sec and found arcs in a high fraction of clusters with $L_x > 10^{45}$ ergs/sec and no arcs in clusters with $L_x < 4 \times 10^{44}$ ergs/sec. Zaritsky & Gonzalez (2003) searched for arcs in 44 optically selected clusters ($0.5 \leq z \leq 0.8$), from a list ranked by surface brightness, finding arcs in two clusters. Gladders et al. (2003) searched ≈ 900 optically selected clusters ($0.3 \leq z \leq 1.4$), ranked by a galaxy overdensity parameter, finding arcs in 8 clusters, with none at $z < 0.64$. Sand et al. (2005) used a very different technique, searching for arcs in the heterogeneous sample of clusters that have been observed with HST; out of 128 clusters ($0.1 \leq z \leq 0.78$) 45 had tangential arcs, although it is worth noting that many of the clusters were targeted by HST precisely because of known arcs. It is possible to compute how many arcs found in high quality images would be found in images of lesser quality, and we will perform such a comparison. The results so far would suggest looking for arcs in clusters with high x-ray luminosity or high redshift. Luppino et al. (1999) found a higher frequency of arcs in high L_x clusters, which since the bremsstrahlung emission in clusters is proportional to n_e^2 suggests arcs are found preferentially in the highest density clusters. Gladders et al. (2003) found a higher frequency of arcs in higher redshift clusters, which suggests either an evolution of cluster structure in a way not fully understood or perhaps that the sources lensed are predominately at a higher redshift where the cross section is much higher for $z \sim 0.7$ clusters than for $z \sim 0.3$ clusters (Ho & White 2005). Observationally, however, it is clear that the dominant observational variables for successful arc detection is limiting surface brightness and especially seeing.

The Sloan Digital Sky Survey (York et al. 2000) to date has produced a multiband

imaging of 8000 sq-deg of the northern sky along with an associated catalog of 1,048,496 spectra of which 674,749 are galaxies (SDSS Collaboration 2006). It has proven useful as a data set for gravitational lens searches. An example is the the multiply-lensed quasar searches of Pindor et al. (2003) and Oguri et al. (2006), which use the imaging data to select for quasar-colored objects that are larger than a PSF, or groupings of quasar-colored objects in a small area. A second example of lens searches in the SDSS data uses the large SDSS spectroscopic data set. Bolton et al. (2006) searched red galaxy spectra for indications of a second, higher redshift nebular emission spectrum. This locates strongly-lensed background galaxies, which are revealed as arcs after galaxy subtraction techniques on HST ACS images. Our program is a search for strongly-lensed background galaxies behind clusters; that is, a search for giant arcs. Our ability to locate gravitational arcs in the SDSS images is demonstrated by recovering arcs observed by other surveys and by the discovery of new gravitational arcs (see Fig.1, Appendix A, and Allam (2006)).

Our analysis consists of a search for giant gravitational arcs produced in a mass estimate sorted sample of galaxy clusters detected in the SDSS imaging data. Our imaging data does not have the depth or seeing of previous searches, but it does have the twin features of homogeneity and of great sky coverage. This results in our ability to greatly increase the numbers of clusters searched. The search reported here totals 825 clusters, comparable to the largest previous search. We intend, in a future paper, to decrease the mass threshold down to the poor group range in order to search tens or hundreds of thousands of locations. Furthermore, the redshift range of the cluster catalog we have searched is predominately $0.1 \leq z \leq 0.3$, a range poorly covered by previous searches.

2. The Data

The data set we use is the SDSS data release 5 SDSS Collaboration (2006). This is an u,g,r,i,z imaging survey that trades a relatively shallow exposure- 55 seconds on a 2.5m telescope resulting in point sources detected repeatably at 95% confidence level at $g = 22.2$ and $i = 21.3$ (AB)- for a very wide area: 8000 sq-degrees or 20% of the total sky. Koester (2006a) used this data to construct a cluster catalog containing 12,875 rich clusters and two orders of magnitude more clusters of lower mass.

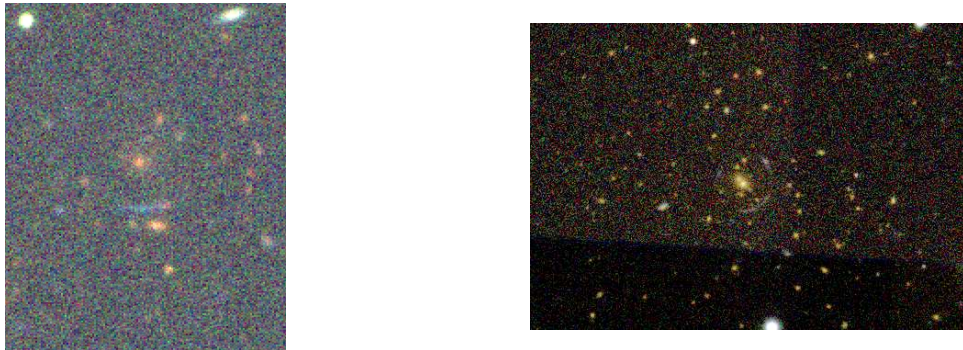


Fig. 1.— On the left, the SDSS image of the RCS1419.2+5361 cluster. The arc was discovered by visual inspection of the RCS cluster sample Gladders et al. (2003) and is clearly visible in this image composed by the g , r and i filters. On the right, Hall’s arc (see appendix), serendipitously discovered in the SDSS data. It, too, is clearly visible in the gri image. These observations, together with the recent discovery of two new arc systems Allam (2006), demonstrate the ability of SDSS to detect this type of object.

2.1. The Cluster Sample

The cluster catalog was constructed using the maxBcg algorithm. This is a red-sequence locating technique that has shown completeness levels of 90% at $0.1 \leq z \leq 0.3$ and down to $N_g = 10$. N_g is the number of red galaxies on the E/S0 red sequence down to $0.4L^*$ within $1h^{-1}$ Mpc and correlates well with mass. A detailed description of the maxBcg technique is discussed in Koester (2006b). The catalog we used in this work was created using an earlier version of the algorithm (see, e.g., Hansen et al. (2005)).

One of the defining features of red sequence methods is that projection effects are present only at a minimal level: if the clusters differ by $\Delta z < 0.05$ then they can be confused as a single object. The resulting purity (lack of false positives) is $\approx 95\%$ and completeness (lack of false negatives) is $\approx 85\%$ above $1 \times 10^{14} M_\odot$, as determined by running this algorithm on mock catalogs (Koester 2006a).

We selected a sample of 825 clusters with $N_g \geq 20$, approximately 50% of the $N_g \geq 20$ clusters in our sample. The whole sample was not searched for a variety of technical reasons, but lack of a complete sample is not important for the results of this paper. The distribution of g-band seeing of the cluster images is shown in Fig. 2 and has a mean of $1.44''$: this is important because it is the single dominating factor in our ability to detect arcs. The redshift distribution is shown in Fig. 3. The most massive of the clusters in our sample are presented Table 5, and the entire table is available electronically.

While we do not use the masses of the clusters directly in this work, we do have a mass calibration albeit one that is preliminary. A calibration of N_g to velocity dispersion and weak lensing gives $\sigma_v = 85N_g^{0.6}$ km/s (see Bahcall et al. (2003); the relation we use is slightly updated from the relation given there). Modeling the cluster as a single isothermal sphere the mass can then be calculated as

$$M_{200} = \left(\frac{\sigma_v}{\sigma_0}\right)^3 \sqrt{\delta_c E(z) H_0} \quad 10^{15} M_\odot, \quad (1)$$

where $E(z) = \sqrt{\Omega_\Lambda + \Omega_m(1+z)^3}$, δ_c is ???, H_0 is the Hubble constant, and Ω_m and Ω_Λ are the energy density of normal matter and the cosmological constant, respectively, in units of the critical density. This calibration has a significant scatter. Indirect methods, such as a) running the cluster finding algorithms in mock catalogs based on N-body simulations and b) measuring the higher moments of the velocity distributions of galaxies in stacked cluster samples, suggest that the scatter is $\approx 40\%$ in $\log M_{200}$ at high N_g and increases to lower N_g . A more sophisticated calibration using weak lensing measurements of the full maxBcg catalog is in preparation Sheldon (2006). In future papers we expect to use the current maxBCG catalog and mass calibrations.

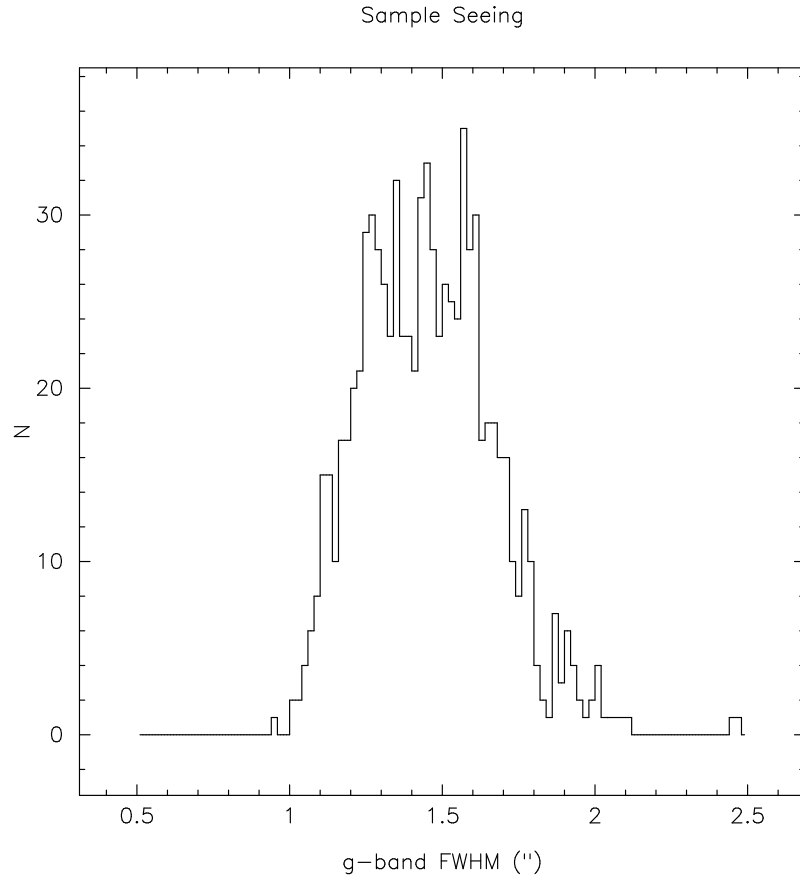


Fig. 2.— The g-band seeing distribution for the SDSS images of the 825 clusters inspected for this work. The distribution is well fit by a gaussian of mean 1.44" and standard deviation 0.20".

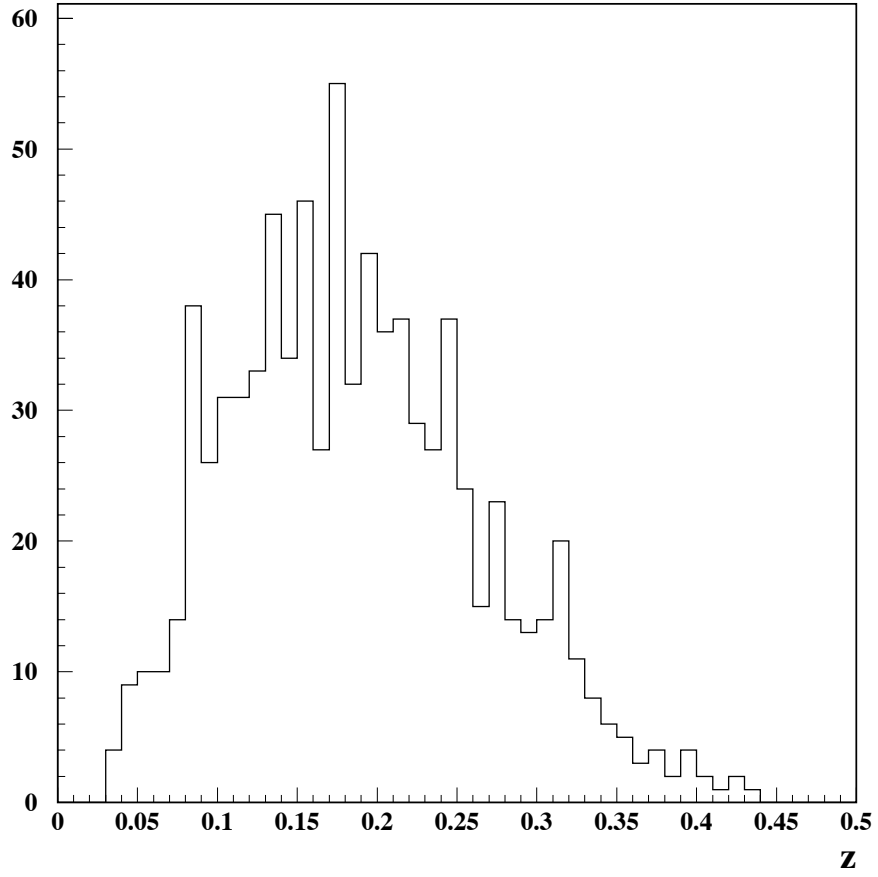


Fig. 3.— The redshift (z) distribution for the 825 clusters inspected for this work. We have large statistics in the range $0.1 < z < 0.3$.

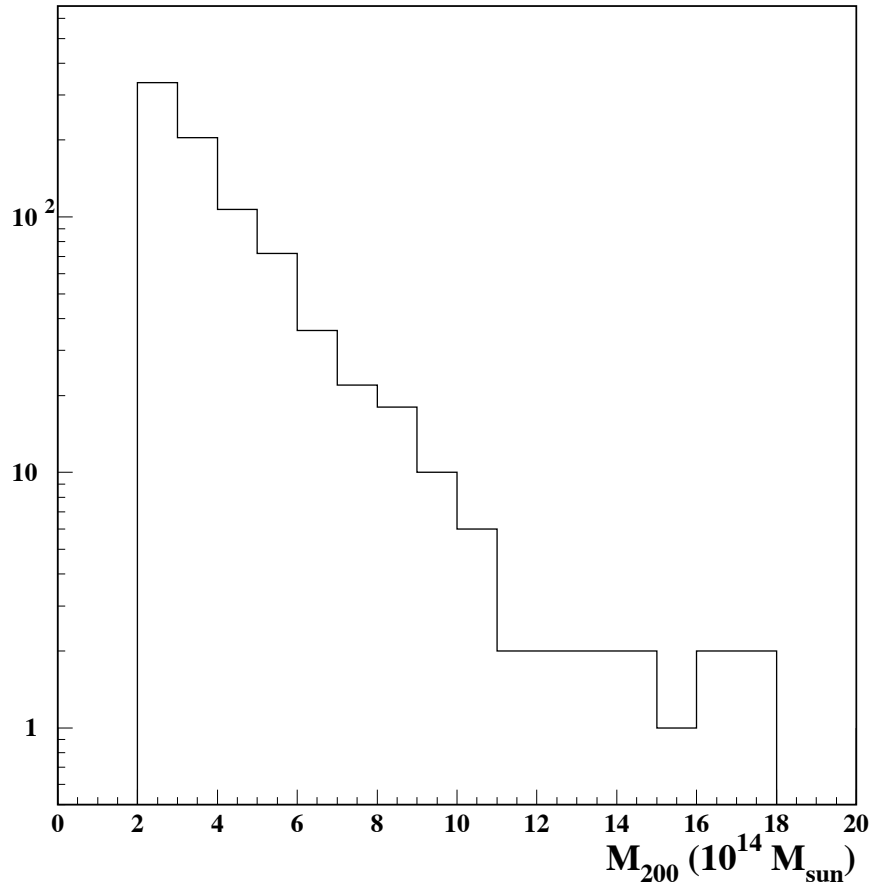


Fig. 4.— Mass distribution in our sample of inspected clusters.

3. Search by Visual Inspection

All the previous arc surveys use visual inspection to locate arc candidates, which are then usually followed up with deeper imaging in better seeing.

The SDSS images of the 825 selected clusters sample were visually inspected for arcs. For each cluster, an image was built covering an angle corresponding to a physical scale of 1 Mpc (assuming $H_0 = 100$ km/s, $\Omega_m = 0.3$ and $\Omega_\Lambda = 0.7$). This was done using the SDSS coadding code. The inspector was then presented with 4 simultaneous images: grayscale images of the g , r and i bands and a color image that combines the three bands. The grayscale images were displayed using an histogram equalization algorithm while the color image was displayed in a fixed surface brightness range. A single author of this work (T.L.) scanned the 825 images while three other authors inspected images of the 300 highest N_g clusters in the sample. Candidates were recorded for later consideration.

3.1. Visual Inspection Selection Function

A selection function is a prerequisite for a serious use of statistics of arcs to pursue cosmology. In order to calculate a selection function for our arc search, simulated arcs were added to a fraction of the images in our cluster sample. These objects were included before the images were inspected for arcs, and without the knowledge of the scanner doing the visual inspection. The added arcs were a section of a circle and centered on the brightest cluster galaxy, as identified by the maxBcg algorithm. We added the arcs with a distribution of surface brightnesses and length vs. width ratio (l/w) in order to have a selection function showing the dependence on these arc parameters. The simulated arcs were assumed to have a flat spectrum, which makes them in general bluer than the cluster galaxies (this is typically true for the real observed gravitational arcs from other surveys). The typical length for the simulated arcs was $l \approx 10''$, and they were inserted in the images at $1''$ - $2''$ from the cluster brightest cluster galaxy. The selection functions obtained with the technique are presented in Fig. 5 and Fig. 6.

For our survey, the detection efficiency reaches 50% at 24.8 mag/arcsec² in g-band and for $l/w \approx 10$. The efficiency does not reach 100% even for high l/w ratio, high surface brightness arcs. The dominant cause of missed arcs is the blending of arcs with galaxies and stars on the images. If the surface brightness for the arc is high enough, it can be detected despite blending with a star or cluster galaxy. The measurement of this selection function suffers from low statistics, because we decided not to populate a significant fraction of our images with simulated arcs.

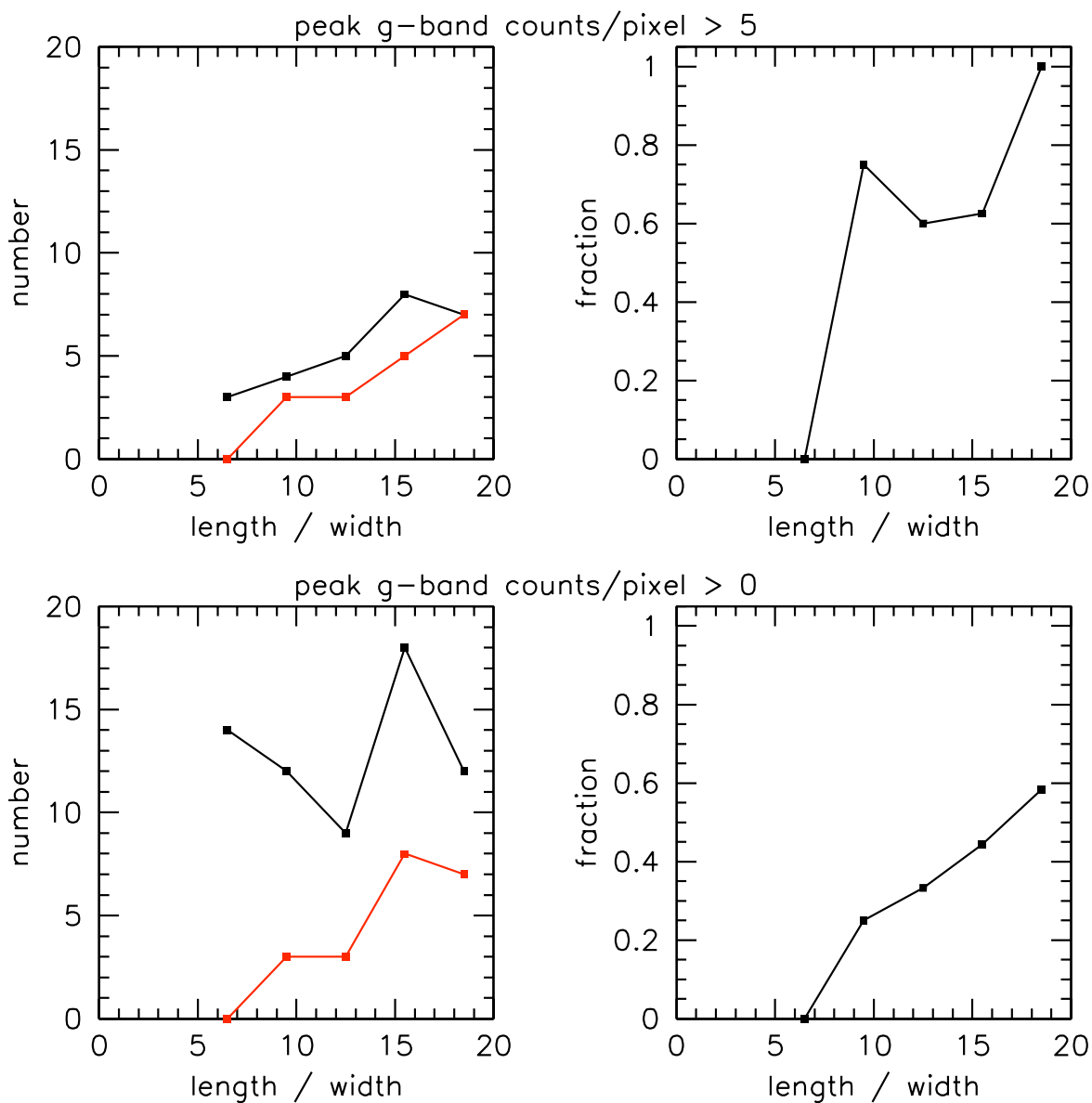


Fig. 5.— Efficiency for finding simulated arcs as a function of l/w . The panels on left show the number of simulated arcs included in the images (black), and the number of those recovered by the visual inspection (red). The panels on the right show the efficiency for recovering the simulated arcs. The top line shows the results for arcs with more than 5 counts/pixel as the maximum brightness of the simulated arc (conversion of counts per pixel to surface brightness is shown in Fig. 6) and the bottom line shows the efficiency for the whole sample.

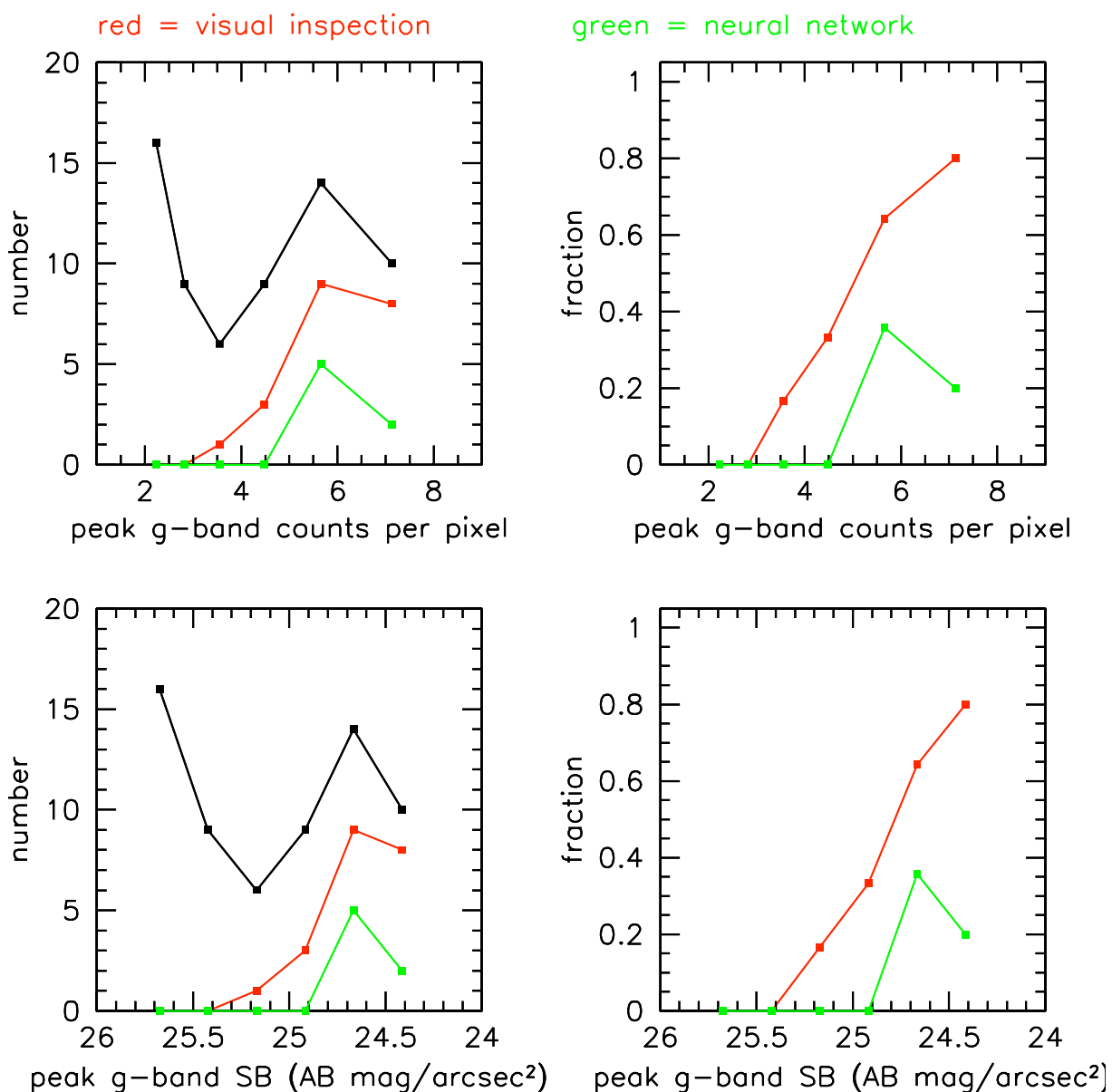


Fig. 6.— Efficiency for finding simulated arcs as a function of g-band peak surface brightness. The panels on the left show the number simulated arcs included in the images (black), the number of those recovered by the visual inspection (red) and the number recovered by the automated search (green). The panels on the right show the efficiency for recovering the simulated arcs.

4. Search by Algorithm

While arc-finding algorithms have been published previously (Lenzen et al. 2004; Horesh et al. 2005), we are not aware of an arc search that has been performed using an algorithm. Clearly if we are to examine 10^5 clusters we will need to use an algorithm (as opposed to a human eye inspection, which one author (JTA) refuses to call an algorithm). We have developed such an algorithm, based on ideas taken from related techniques used in experimental particle physics for tracking particles in cloud and bubble chambers. In this work our main goal is to set a benchmark comparison between a simple algorithm for arc detection and a visual inspection.

4.1. The Algorithm

The algorithm is composed of three steps: image preparation, candidate preselection, and final arc selection.

Step 1 is image preparation, where we scale the g, r, i images by the variance of their respective sky, normalize the variances to 1.0, average the three images together, and then run SEXtractor to produce an object image. This step is intended to enhance the signal-to-background ratio of the arc-like objects. The averaging of the variance normalized images follows the ideas of Szalay et al. (1999), and the intent is to produce an image where the pixel values are a χ^2 of the hypothesis that the pixel consists of only sky. The SEXtractor (Bertin & Arnouts 1996) produced object image has eliminated isolated pixels above threshold (due to noise) that do not belong to any object, retaining only pixels belonging to objects detected above threshold. We perform a deblending of the SEXtractor objects by separating as different objects every group of pixels above threshold but that are separated from the rest of the object by more than 2 pixels.

Step 2 is candidate preselection, where the basic shape of the candidates is characterized by measuring the major and minor main axis of each object and objects that show elongated shapes are kept for further study. The major axis (r_1) is defined as the largest distance between any pair of the N pixels belonging to the object, and the minor axis (r_2) is defined as the maximum distance between pixels perpendicular to the main axis. Elongated objects, where $r_1/r_2 \geq 1.4$, are chosen for further analysis. Step 2 simply reduces the number of objects to be studied, in order to reduce computation time per image. It is designed to be efficient (keeping $\approx 100\%$ of the arc-like objects) and provide about a factor of 100 in rejection against the rest of the objects detected by SEXtractor.

Step 3 is final arc selection, where the remaining objects have their radius of curvature

measured and that plus other parameters measured in step 2 become the input for a neural net (NN) trained to select simulated arcs. The output of this NN is used to determine if an object is a good arc candidate. The radius of curvature (R) is measured using a least squares fit. The selection of good arc candidates then uses the following quantities:

- $2\pi/R$: the fraction of circumference covered by arc. This is typically > 0.2 for objects with significant curvature.
- $N/(\pi R^2)$: the fraction of circle area covered by pixels above threshold. This is typically < 0.15 for good candidates.
- χ^2/N : the goodness of fit.
- r_1 : the size of the long axis: This ensures significant size for the candidates, > 20 pixels.

The 4 quantities described above are then presented to a NN with 8 nodes in a hidden layer and the output trained (back propagation) to identify simulated arcs. The NN was trained in a sample of 100 bright simulated arcs, where the peak brightness of 20 counts in g-band.

4.2. Algorithm Selection Function

The efficiency obtained with this algorithm is somewhat lower than that seen in the human scan and is shown in Fig.6. The detection efficiency reaches 40% at 24.7 mag/arcsec² in g-band and for $l/w \approx 10$; the curve is consistent with the eye scan curve shifted to a brighter SB by ≈ 0.4 mags. More development will be needed to bring this algorithm to the level of efficiency of visual inspection. However, this benchmark point provides a basis for the comparison of the human search and a simple algorithm search over the same sample.

5. Candidate Followup

The six best candidates, all from the visual inspection, were selected for followup.

These six arc candidates were observed using the SPICAM imager on the Apache Point Observatory 3.5 meter telescope. Images were recorded in the Sloan g, r, and i filters. The observation date was April 29-30, 2006, which was dark time. Table 1 shows the amount of time spent observing each object with the three filters. The images were reduced using bias subtraction and flat-fielding determined separately for each filter. The images were

registered and coadded. Typical individual image point spread functions ranged from 1.1" to 1.5".

The candidates were inspected by the authors and discarded based on judgements that they were most likely “junk” or edge on galaxies. Room for improvement in this system exists and we plan on putting into place a set of criteria for systematic followup. The criteria useful for SDSS data are obvious from an examination of Fig. 1: l/w , surface brightness, radius of curvature, and color.

We found no convincing candidates.

6. Results of the Searches

Our survey of 825 SDSS galaxy clusters resulted in no convincing candidates for giant gravitational arcs.

The selection function we have computed shows that we are $\geq 50\%$ efficient at $SB \leq 24.8$ mags/arcsec² and for $l/w \geq 10$. The latter, given our mean seeing of 1.4" corresponds to arcs longer than 14". Fig. 7 shows the surface brightness of the arcs found in by Lynds & Petrosian (1989, in seeing of $\sim 1.0''$), by Luppino et al. (1999, $\sim 0.90''$, their table 2) by Zaritsky & Gonzalez (2003, $\sim 0.55''$), and by Gladders et al. (2003, $\sim 0.85''$). These are all the ground based surveys, and no attempt to homogenize seeing has been made. The surface brightnesses have been converted to the AB system from the Vega system. We assume that the arcs have flat spectra so that no change is necessary for differing bandpasses. We see on that figure that our surface brightness limit is in fact exceeded by the majority of these arcs- it is the relatively large PSF of the SDSS data that limits us to $l/w \geq 10$ (and reduces the observed surface brightness) that limits our search. Still, the arcs that we locate will be quite long arcs with high surface brightness, and thus will be interesting objects for followup.

6.1. Upper Limits to Observable Arc Production

We use this result to establish an upper limit on the production of observable giant arcs by our galaxy clusters. Assuming Poisson statistics, an observation of 0 arcs in a redshift bin indicates that if the experiment is repeated the probability of observing < 3 arcs is 95%. We can therefore set 95% confidence level upper limits of the probability of observing an arc in our sample of clusters as a function of redshift. This is shown in Fig. 8. It should be noted that this limit corresponds to arcs observable by SDSS according to the efficiency for detection shown in Fig. 5 and Fig. 6. The lower panel in Fig. 8 corresponds to the more

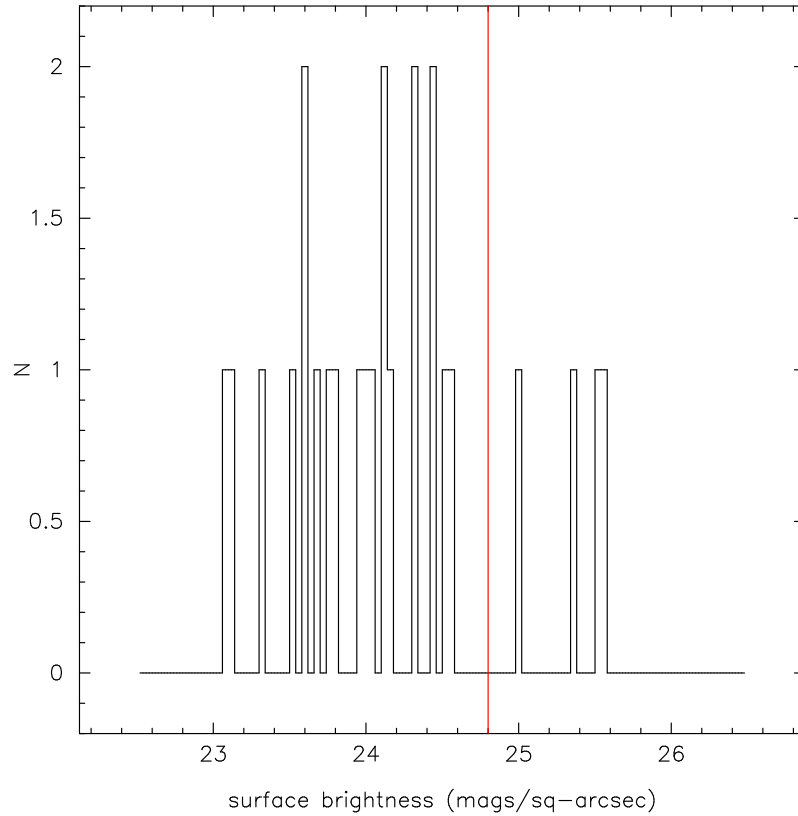


Fig. 7.— The surface brightnesses of the arcs found in previous ground based searches. The surface brightness is reported in the AB system and given the assumption of a flat spectrum arc we need not report the bandpass, though the data were in fact observed through a variety of filters: B,V,R,I. The vertical red line is the 50% efficiency limit of our visual search selection function. The observed surface brightness for arcs that are unresolved in width is a function of the seeing obtained, and the data here, while all ground based, has a variety of seeing. All are better than our sample’s mean seeing of $1.4''$, so if this plot were homogenized to the SDSS seeing most, not all, of the arcs would be below our surface brightness limit. Seeing is the dominant limiting factor in our efficiency.

massive clusters in our sample and from the plot it is clear that we only have statistics for a significant limit in the range $0.1 < z < 0.3$.

6.2. Comparison With Previous Work

In order to understand the compatibility of our results with previous arc searches, we perform a direct comparison with these searches over similar redshifts. The sample of X-ray luminous galaxy clusters constructed by Smith et al. (2005) is a good place to start. This sample has a total of 10 rich clusters with $M_{200} < 4 \times 10^{14} M_{\odot}$ at $0.17 \leq z \leq 0.26$, where the mass is estimated from X-ray luminosities (Allen et al. 2003). The sample was imaged with HST and the geometrical properties of the arcs are published by Sand et al. (2005). In order to estimate the expected number of arcs observable for SDSS the parameters for the arc candidates were degraded from those observed in HST imaging (with a typical PSF of $0.15''$) to the image quality of SDSS (with a typical PSF of $1.4''$). This conversion is done assuming that the arc is well resolved in HST imaging, i.e., that the width is entirely due to the object, not the PSF. The width is then increased by adding in quadrature the average seeing for SDSS, effectively reducing l/w ratio. The increased width results in an increased area of the object, which translates into a change in surface brightness. Of the arc candidates observed with HST in these clusters, only 3 will remain with $l/w > 10$ after degradation to SDSS seeing. Of the surviving arcs only 1 will have a surface brightness inside our detection limit. Thus this sample of Smith et al. (2005) gives a 10% probability of having an arc observable by SDSS for clusters with $M_{200} < 4 \times 10^{14} M_{\odot}$ and $0.15 < z < 0.3$. This result lies inside the 95% C.L. presented in Fig. 8.

A similar comparison can be done with the EMSS (Luppino et al. 1999) sample of 38 x-ray selected clusters with $L_x \geq 2 \times 10^{44}$ ergs/sec at $0.15 \leq z \leq 0.82$. As before, the parameters for the arcs were transformed into expected parameters for SDSS using the seeing for each arc observation. After this, no arc in this sample is expected to be observable in SDSS imaging. Again, giving a result consistent with our observation.

The results obtained in this work are also consistent with the observation made in a previous search for giant gravitational arcs in the RCS (Gladders et al. 2003). The RCS cluster sample covers a redshift region $0.35 < z < 0.95$, and after human inspection of approximately 900 clusters with $M_{200} < 4 \times 10^{14} M_{\odot}$, 3 strong lensing systems with giant arcs were found, all of them with $z > 0.60$. The result from RCS indicated a small probability of a low redshift cluster to produce an arc, compared with a similar mass cluster at higher redshift. The clusters used for the arc search in this work have a lower redshift (with the bulk of the clusters with $0.1 < z < 0.3$) and the null result is also consistent with the low

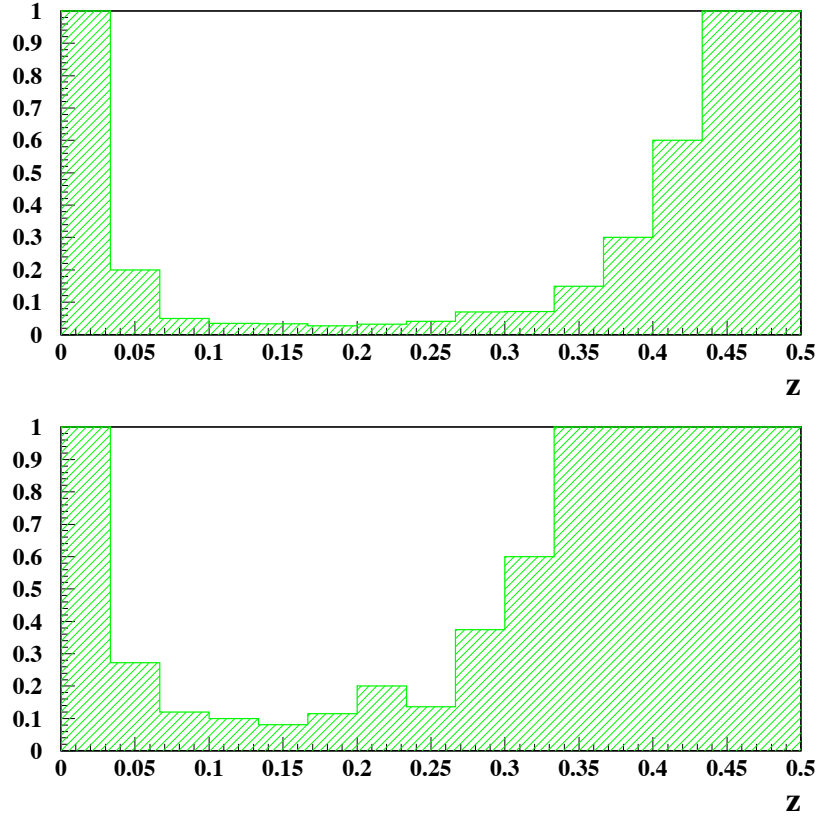


Fig. 8.— The 95% C.L. upper limit for the probability for a cluster producing a gravitational arc visible in SDSS imaging assuming Poisson statistics in our sample of 825 clusters. The top panel shows the limit as a function of redshift for $2 < M_{200}/10^{14}M_{\odot} < 4$ and the bottom panel for $M_{200}/10^{14}M_{\odot} < 4$.

redshift clusters being less efficient in the production of arcs.

We are aware of 4 giant arcs in the single pass SDSS imaging, one first discovered by the RCS, one described in the appendix, and two that will be described in Allam (2006). Three of the arcs are lensed by clusters with $N_g \sim 10 - 20$, beneath the threshold of our current work, and these have $0.35 \leq z \leq 0.45$, beyond our catalog redshift limits but well within the reach of SDSS cluster finders. The other is RCS1419.2+5326 at $z = 0.64$: our cluster finders can find these kinds of objects, but with $N_g \sim 5$ (as observed by SDSS, the real N_g would be much higher) the catalogs are nowhere near the 90% efficiency level of the $z < 0.3$ catalogs; one might imagine the efficiency is on the order of 1 – 5%. It is worth noting that the two high surface brightness arcs found by Lynds & Petrosian (1989) are just south of the limits of the SDSS strip 82. Had both clusters been 1 degree farther north, they likely would have been found in our survey.

7. Summary

The potential for observing arcs in SDSS imaging has been demonstrated by the observation of known arcs systems in the multiband imaging of the survey (see Fig.1) and by the discovery of new arcs (Allam 2006). In this work, we presented a systematic search for gravitational arcs in a sample of SDSS clusters. A total 825 clusters with $M > 2 \times 10^{14} M_\odot$ have been visually inspected for arcs, and also processed with an automated arc search algorithm. The efficiency of the arc detection (in both techniques) has been quantified by introducing simulated arcs into the inspected images. The results indicate significantly higher efficiency for the hand scan, and point to the need for developing a more efficient algorithm for a automated search. No gravitational arcs were seen in the sample of clusters analyzed. This result is consistent with previous surveys done in similar redshift region, and reinforces the evidence of evolution of the number of arcs per cluster as a function of redshift (for a fixed cluster mass) as seen in the RCS sample (Gladders et al. 2003).

8. Acknowledgements

Funding for the SDSS and SDSS-II has been provided by the Alfred P. Sloan Foundation, the Participating Institutions, the National Science Foundation, the U.S. Department of Energy, the National Aeronautics and Space Administration, the Japanese Monbukagakusho, the Max Planck Society, and the Higher Education Funding Council for England. The SDSS Web Site is <http://www.sdss.org/>.

The SDSS is managed by the Astrophysical Research Consortium for the Participating Institutions. The Participating Institutions are the American Museum of Natural History, Astrophysical Institute Potsdam, University of Basel, Cambridge University, Case Western Reserve University, University of Chicago, Drexel University, Fermilab, the Institute for Advanced Study, the Japan Participation Group, Johns Hopkins University, the Joint Institute for Nuclear Astrophysics, the Kavli Institute for Particle Astrophysics and Cosmology, the Korean Scientist Group, the Chinese Academy of Sciences (LAMOST), Los Alamos National Laboratory, the Max-Planck-Institute for Astronomy (MPIA), the Max-Planck-Institute for Astrophysics (MPA), New Mexico State University, Ohio State University, University of Pittsburgh, University of Portsmouth, Princeton University, the United States Naval Observatory, and the University of Washington.

A. Appendix: Hall’s Arc

We report here an arc discovered serendipitously by one of us (P.B.H) in 2004. It is widely known inside the SDSS Collaboration but has not been published previously. The purely serendipitous discovery was made during inspection of the images of spectra classified UNKNOWN (the initial reduction of the SDSS spectrum had bad spectrophotometry and could not be classified). There is a cluster clearly visible in the images: the BCG has a SDSS spectrum and is at $z = 0.44$, and it is coincident with NVSS J014656-092952. The SDSS spectrum shows two objects superimposed, the $z = 0.44$ galaxy and a star- the latter is what the SDSS pipeline reports.

We ran the maxBcg code at the position of the BCG and measured $N_g = 12$, but this is a lower limit. The cluster is above the redshift where the N_g is complete- at this redshift two effects compromise the N_g measurement: 1) $0.4L^*$ is fainter than the useful limiting magnitude of the SDSS, and 2) the colors of objects near $0.4L^*$ become noisy enough to scatter outside the color box used to determine cluster membership. A correction must be applied to N_g for these effects. As we are not attempting to use this arc in our analysis we defer the measurement of the corrected N_g to a later paper. We have tabulated our information about the cluster in table 2.

There are three arcs. The longest one was split by the SDSS pipeline Photo into two objects, a and b. We report on the object parameters in table 3. Three of the four objects have photometric redshifts near 0.6; the fourth is 2σ away. We measured the parameters of the three arcs in the SDSS g-band image. These are listed in table 4. It is likely that we would have found this arc in our survey (if it had been in our sample catalog) because it is remarkably clean: there are no stars or cluster galaxies that are projected onto the images

of the arcs.

Table 1. Candidate Observations

Name	RA	Dec	z	g (min)	r (min)	i (min)
SDSS+139.5+51.7+0.24	09:17:59.5	51:42:06	0.24	15	5	5
SDSS+184.4+3.6+0.08	12:17:28.0	03:36:17	0.08	15	5	5
SDSS+117.7+17.7+0.19	07:50:48.9	17:40:43	0.19	15	5	5
SDSS+175.3+5.8+0.12	11:41:13.5	05:48:28	0.12	15	5	5
SDSS+205.5+26.4+0.10	13:41:49.1	26:22:25	0.10	15	5	5
SDSS+139.1+5.9+0.14	09:16:21.3	05:53:18	0.14	15	5	5

Note. — Spicam observations. The redshifts quoted for the clusters are photometric redshifts from the maxBcg algorithm and have a dispersion of $\sigma_z = 0.015$.

Table 2. Hall’s Arc: the Cluster

Name	RA	Dec	z	N_g
SDSS+26.733-9.497+0.44	01:46:56.00	-09:29:52.4	0.44	$\geq 12^a$

^aLower limit; see text.

Table 3. Hall’s Arc: Positions, Magnitudes, and Photo-zs

Arc	RA	Dec	g	u-g	g-r	r-i	i-z	$z_{\text{phot}}^{\text{b}}$
1a	26.73210	-9.50009	21.85 ± 0.15	1.3 ± 1.4	0.57 ± 0.21	0.68 ± 0.19	0.09 ± 0.51	0.62 ± 0.15
1b	26.73051	-9.49967	21.81 ± 0.21	0.39 ± 0.92	0.75 ± 0.27	0.63 ± 0.22	-1.8 ± 2.6	0.57 ± 0.23
2	26.73063	-9.49525	21.66 ± 0.10	0.45 ± 0.46	0.53 ± 0.14	0.73 ± 0.12	0.29 ± 0.28	0.67 ± 0.08
3	26.73641	-9.49673	21.77 ± 0.15	0.66 ± 0.81	0.03 ± 0.27	0.15 ± 0.39	-1.1 ± 2.1	0.08 ± 0.27

Note. — SDSS data. We retain the SDSS decimal degrees convention for RA and Dec. The magnitudes and colors are SDSS model magnitudes and are corrected for extinction (see SDSS Collaboration 2006, and references therein).

^bthe mean of the SDSS photoz and photoz2 (SDSS Collaboration 2006).

Table 4. Hall’s Arc: Arc Parameters

Arc	l	obs. l/w	mean SB_g
1	17.2''	11.2	24.5
2	10.0''	6.5	24.6
3	3.8''	2.5	23.7

Note. — g-band SDSS data measurements. The g-band PSF is 1.53''.

Name	RA	DEC	z	N_{gals}	M_{200}
SDSS+239.6+27.2+0.11	239.634	27.1808	0.109	94.	31.2
SDSS+230.6+27.7+0.08	230.6	27.7144	0.083	88.	28.1
SDSS+213.6-00.3+0.13	213.618	-0.3301	0.133	69.	17.7
SDSS+117.7+17.7+0.19	117.721	17.6768	0.192	68.	16.7
SDSS+258.2+64.0+0.08	258.227	63.9924	0.081	67.	17.2
SDSS+227.8+05.8+0.08	227.75	5.7828	0.081	65.	16.3
SDSS+197.9-01.3+0.20	197.886	-1.3329	0.203	65.	15.3
SDSS+234.9+34.4+0.25	234.893	34.4369	0.249	63.	14.1
SDSS+250.1+46.7+0.25	250.098	46.7028	0.242	62.	13.7
SDSS+110.4+36.7+0.15	110.36	36.7383	0.148	62.	14.4
SDSS+227.6+33.5+0.12	227.584	33.486	0.116	59.	13.4
SDSS+250.8+13.4+0.20	250.843	13.363	0.199	58.	12.5
SDSS+126.3+47.1+0.13	126.32	47.1424	0.129	58.	12.9
SDSS+203.8+41.0+0.26	203.818	41.0132	0.264	55.	10.9
SDSS+139.5+51.7+0.24	139.481	51.7163	0.236	54.	10.7
SDSS+255.7+34.1+0.11	255.69	34.0611	0.109	54.	11.5
SDSS+228.8+04.4+0.11	228.823	4.397	0.107	53.	11.1
SDSS+137.3+11.0+0.18	137.329	10.9857	0.179	53.	10.7
SDSS+184.4+03.6+0.08	184.381	3.6157	0.089	52.	10.9
SDSS+216.5+37.8+0.16	216.475	37.7915	0.164	50.	9.7

Table 5:: List of the most 20 most massive inspected clusters in our sample. The full sample is available electronically.

REFERENCES

- Allam, S. S. 2006, in preparation
- Allen, S. W., Schmidt, R. W., Fabian, A. C., & Ebeling, H. 2003, *MNRAS*, 342, 287
- Bahcall, N. A. et al. 2003, *ApJS*, 148, 243
- Bartelmann, M., Huss, A., Colberg, J. M., Jenkins, A., & Pearce, F. R. 1998, *A&A*, 330, 1
- Bertin, E., & Arnouts, S. 1996, *A&AS*, 117, 393
- Bolton, A. S., Burles, S., Koopmans, L. V. E., Treu, T., & Moustakas, L. A. 2006, *ApJ*, 638, 703
- Dalal, N., Holder, G., & Hennawi, J. F. 2004, *ApJ*, 609, 50
- Gilmore, J., & Natarajan, P. 2006, astro-ph/0605245
- Gladders, M. D., Hoekstra, H., Yee, H. K. C., Hall, P. B., & Barrientos, L. F. 2003, *ApJ*, 593, 48
- Hansen, S. M., McKay, T. A., Wechsler, R. H., Annis, J., Sheldon, E. S., & Kimball, A. 2005, *ApJ*, 633, 122
- Ho, S., & White, M. 2005, *Astroparticle Physics*, 24, 257
- Horesh, A., Ofek, E. O., Maoz, D., Bartelmann, M., Meneghetti, M., & Rix, H.-W. 2005, *ApJ*, 633, 768
- Koester, B. 2006a, in preparation
- . 2006b, in preparation
- Lenzen, F., Schindler, S., & Scherzer, O. 2004, *A&A*, 416, 391
- Luppino, G. A., Gioia, I. M., Hammer, F., Le Fèvre, O., & Annis, J. A. 1999, *A&AS*, 136, 117
- Lynds, R., & Petrosian, V. 1989, *ApJ*, 336, 1
- Oguri, M., Lee, J., & Suto, Y. 2003, *ApJ*, 599, 7
- Oguri, M. et al. 2006, astro-ph/0605571
- Pindor, B., Turner, E. L., Lupton, R. H., & Brinkmann, J. 2003, *AJ*, 125, 2325

Sand, D. J., Treu, T., Ellis, R. S., & Smith, G. P. 2005, ApJ, 627, 32

SDSS Collaboration. 2006, in preparation

Sheldon, E. 2006, in preparation

Smith, G. P., Kneib, J.-P., Smail, I., Mazzotta, P., Ebeling, H., & Czoske, O. 2005, MNRAS, 359, 417

Szalay, A. S., Connolly, A. J., & Szokoly, G. P. 1999, AJ, 117, 68

Wambsganss, J., Bode, P., & Ostriker, J. P. 2004, ApJ, 606, L93

York, D. G. et al. 2000, AJ, 120, 1579

Zaritsky, D., & Gonzalez, A. H. 2003, ApJ, 584, 691